Subgap states and quantum phase transitions in one-dimensional superconductor–ferromagnetic insulator heterostructures

Javier Feijoo [1,2] Aníbal Iucci [1,2] and Alejandro M. Lobos [3,4]
[1]*Instituto de Física La Plata - CONICET, Diag 113 y 64 (1900) La Plata, Argentina*
[2]*Departamento de Física, Universidad Nacional de La Plata, cc 67, 1900 La Plata, Argentina*
[3]*Facultad de Ciencias Exactas y Naturales, Universidad Nacional de Cuyo and CONICET, 5500 Mendoza, Argentina*
[4]*Instituto Interdisciplinario de Ciencias Básicas (CONICET-UNCuyo), M5500 Mendoza, Argentina*

(Received 10 January 2023; accepted 30 May 2023; published 7 June 2023)

We theoretically study the spectral properties of a one dimensional semiconductor-superconductor-ferromagnetic insulator (SE-SU-FMI) hybrid nanostructure, motivated by recent experiments where such devices have been fabricated using epitaxial growing techniques. We model the hybrid structure as a one-dimensional single-channel semiconductor nanowire under the simultaneous effect of two proximity-induced interactions: superconducting pairing and a (spatially inhomogeneous) Zeeman exchange field. The coexistence of these competing mechanisms generates a rich quantum phase diagram and a complex subgap Andreev bound state (ABS) spectrum. By exploiting the symmetries of the problem, we classify the solutions of the Bogoliubov-de Gennes equations into even and odd ABS with respect to the spatial inversion symmetry $x \to -x$. We find the ABS spectrum of the device as a function of the different parameters of the model: the length L of the coexisting SU-FMI region, the induced Zeeman exchange field h_0, and the induced superconducting coherence length ξ. In particular we analyze the evolution of the subgap spectrum as a function of the length L. Interestingly, we generically find spin-polarized ABS emerging in the subgap region, which, depending on the ratio h_0/Δ, can eventually cross below the Fermi energy at certain critical values L_c, and induce spin- and fermion parity-changing quantum phase transitions. We argue that this type of device constitute a promising highly-tunable platform to engineer subgap ABS.

DOI: 10.1103/PhysRevB.107.214505

I. INTRODUCTION

The interplay of superconductivity and magnetism at the microscopic scale has attracted a great deal of attention in recent years [1–4]. For instance, the Yu-Shiba-Rusinov (YSR) states [5–7] arising from the exchange interaction of an atomic magnetic moment in contact with a superconductor, have been proposed as fundamental building blocks to engineer quantum devices with topologically nontrivial ground states. In particular, the so-called "Shiba chains" (i.e., one-dimensional arrays of magnetic atoms deposited on top of a clean superconductor) are systems predicted to support Majorana zero modes at the ends of the chain [8–10], and could be used in topologically-protected quantum computation schemes. Low-temperature scanning-tunneling microscopy (STM) experiments have confirmed the presence of intriguing zero-energy end modes [11–17].

Other systems where the competition of superconductivity and magnetism at the nanoscale generates exotic subgap states are superconductor (SU)–ferromagnet (FM) heterostructures, such as SU-FM-SU Josephson junctions and SU-FM proximity devices [18–20]. More recently, a novel class of hybrid device, i.e., semiconductor (SE) nanowire systems combined with superconductors and ferromagnetic insulator (FMI) materials have been fabricated using molecular-beam epitaxy techniques [21–23]. These SE-SU-FMI hybrid structures allow to build nanostructures with specific tailored properties, which are impossible to obtain with the isolated individual components.

Despite the evident differences between the above-mentioned physical systems, from the theoretical perspective they can be described within the same unified theoretical model combining superconductivity and local exchange fields at the microscopic scale. Subgap states generated in these structures are generically referred to as Andreev bound states (ABS), as they emerge due to Andreev reflection processes taking place at the interfaces and/or inhomogeneities of the SU order parameter [19,24]. In this context, YSR states can be considered as a particular class of ABS emerging in atomic-sized heterostructures. In this paper, we will refer to either ABS or YSR states depending on the context, but it should be kept in mind that they are essentially the same type of subgap excitation.

A generic feature of all ABS is that they appear symmetrically around the Fermi level E_F, and localize spatially around the impurity or the FM region. Their energy position within the gap depend on the value of the exchange field and on other experimental parameters. Interestingly, whenever one of these states crosses E_F, a spin- and parity-changing quantum phase transition, usually known as the "$0-\pi$" phase transition, occurs [1,25]. In the case of atomic "Shiba impurities" or ultra-short SU-FM-SU junctions (i.e., junctions in which the length L of the FM region is much smaller than λ_F, the Fermi wavelength of the superconductor [26]), it is customary to

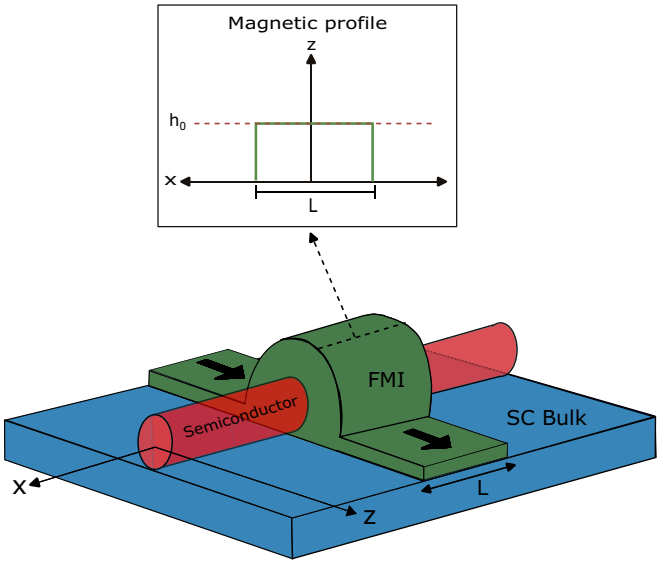

FIG. 1. Schematic representation of the SC-FMI heterostructure.

consider the magnetic scatterer as a *point-like* classical spin $\boldsymbol{S}$ located at the point $\boldsymbol{R}_0$, interacting via a contact *s-d* exchange interaction $H_Z = J(\boldsymbol{r})\,\boldsymbol{S}\cdot\boldsymbol{s}(\boldsymbol{r})$ with the host superconducting electrons [6]. Here $J(\boldsymbol{r}) = J_0\delta(\boldsymbol{r}-\boldsymbol{R}_0)$ is the local exchange potential and $\boldsymbol{s}(\boldsymbol{r})$ is the spin density vector of the electronic fluid. Subsequent theoretical works considered atomic-sized systems with finite- (albeit short-ranged) exchange interactions with spherical symmetry [7,27–29]. In that case, theory predicts the existence of multiple YSR states labeled by their orbital momentum ℓ, a prediction that has been recently confirmed in STM experiments [30–32]. The behavior of subgap states and the associated $0-\pi$ quantum phase transitions has also been studied in the opposite limit $L \gg \lambda_F$ in the context of ballistic SU-FM-SU Josephson junctions with generic spin-dependent fields in the sandwiched region [33–35]. In this case the results differ from the well-known results of atomic-sized YSR states due to the finite extension of the magnetic profile. In particular, the subgap spectrum of long SU-FM-SU junctions with zero phase difference is known to be double degenerate [19,34], showing the inherent complexity of these hybrid heterostructures. On the experimental side, the possibility to engineer and control the position of the subgap states by a modification of the fabrication parameters (e.g., the length L or exchange field h_0 via different FM materials) opens interesting perspectives for potential electronic devices, where the precise knowledge of the subgap spectrum is crucial to control their transport properties.

Motivated by the experimental developments mentioned above, in this paper we study the subgap states emerging in one-dimensional (1D) SE-SU-FMI heterostructures where the SU and the FMI layers simultaneously generate coexisting proximity-induced pairing and exchange interactions over a *finite and arbitrary* length L in the SE nanowire, as schematically shown in Fig. 1. This coexistence is a crucial aspect of this device, which makes it unique and different from the above-mentioned SU-FM-SU junctions, where such overlap occurs only at the SU-FM interface. Our main goal in this paper is to study and understand the behavior of the subgap ABS in this device as a function of the experimentally relevant parameters of the model, i.e., the length L of the FMI region and the magnitude of the induced exchange field h_0. As mentioned above, a device similar to that shown in Fig. 1 has been recently experimentally realized in SE nanowires with epitaxially-grown SU and FMI layers [21–23], and has been further investigated theoretically [36,37]. While the main interest of those works was to design a device with nontrivial topological SU ground state hosting Majorana zero modes, here we will study the regime of parameters favoring a topologically-trivial ground state. As we will show below (see Sec. II), this case is already very complex and rich as a result of the antagonistic SU and FM interactions and, to the best of our knowledge, the detailed behavior of subgap states and the quantum phase diagram emerging in such a system have not been explicitly studied before. Our results indicate the generic presence of spin-polarized ABS, which can induce spin- and parity-changing quantum phase transitions (SP-QPT). Interestingly, recent experimental studies suggest that such spin-polarized ABS have been observed in transport experiments [23].

The article is organized as follows. In Sec. II, we introduce the model representing a 1D SE-SU-FMI hybrid nanowire, discuss the solution to the Bogoliubov-de Gennes equations for the subgap states, and derive a generic equation for the subgap spectrum. In Sec. III, we analyze the results in two specific limits, where we recover well-known results: (a) the semiclassical limit, where the superconducting coherence length ξ is much larger than the Fermi wavelength λ_F, and (b) the atomic YSR limit, in which the exchange-field induced by the FMI region becomes a delta-function potential, i.e., infinitesimally narrow ($L \ll \lambda_F$), and infinitely deep ($h_0 \gg E_F$), in such a way that the product $h_0.L = J$ is kept constant. In both cases, well-known analytical solutions to the subgap spectrum can be recovered. In addition, we numerically solve the characteristic equation for the subgap states and provide a generic description of the subgap spectrum, not restricted to any of these limits. We find a rich behavior of the subgap ABS, where the competing FM exchange and SU pairing interactions give rise to SP-QPT. Finally, in Sec. IV, we present a summary and our conclusions.

II. THEORETICAL MODEL

We focus on the system schematically depicted in Fig. 1, which represents a 1D SE-SU-FMI hybrid nanostructure of total length $L_{\rm w}$, similar to those fabricated in Refs. [21–23]. We model this system with the Hamiltonian $H = H_{\rm w} + H_\Delta + H_Z$, where

$$H_{\rm w} = \sum_\sigma \int_{-\frac{L_{\rm w}}{2}}^{\frac{L_{\rm w}}{2}} dx\, \psi_\sigma^\dagger(x)\left[-\frac{\hbar^2\partial_x^2}{2m^*} - \mu\right]\psi_\sigma^\dagger(x), \tag{1}$$

$$H_\Delta = \Delta \int_{-\frac{L_{\rm w}}{2}}^{\frac{L_{\rm w}}{2}} dx\, [\psi_\uparrow^\dagger(x)\psi_\downarrow^\dagger(x) + \text{H.c.}], \tag{2}$$

$$H_Z = \int_{-\frac{L_{\rm w}}{2}}^{\frac{L_{\rm w}}{2}} dx\, h(x)[\psi_\uparrow^\dagger(x)\psi_\uparrow(x) - \psi_\downarrow^\dagger(x)\psi_\downarrow(x)]. \tag{3}$$

Here $H_{\rm w}$ is the Hamiltonian of a single-channel SE nanowire of length $L_{\rm w}$, in which the fermionic operator $\psi_\sigma(x)$

annihilates an electron at position x with spin projection $\sigma = \uparrow, \downarrow$ and effective mass m^*. The parameter μ is the chemical potential, which can be experimentally varied applying external gates beneath the nanostructure.

The terms H_Δ and H_Z represent, respectively, the proximity-induced pairing interaction encoded by the parameter Δ, and the Zeeman exchange interaction introduced by the FMI and described by a space-dependent exchange field $h(x)$, which we assume oriented along the z direction (see Fig. 1). Moreover, since these interactions are externally induced into the semiconductor, we make the additional assumption that Δ is unaffected by the presence of $h(x)$. Alternatively, one can assume that Δ is already the renormalized value, which takes into account the effect of the FMI, see Refs. [23,36]. In any case, this fact does not affect our conclusions qualitatively. As mentioned before, these two terms can be effectively induced by the presence of epitaxially-grown SU and FMI shells in contact with the SE nanowire [21–23]. It has been experimentally confirmed [22] that the FMI shell (EuS in that case) consists of a single magnetic monodomain, and therefore modeling this layer by the Hamiltonian H_Z is a reasonable approximation. In addition, the epitaxially-generated interfaces are essentially disorder-free, a necessary condition to produce a proximity-induced hard gap [38–40]. This feature allows to neglect the effects of disorder and considerably simplifies the theoretical description. The presence of both, a hard proximity-induced superconductor gap and an effectively induced Zeeman field, in these nanowires have been reported in transport measurements in Refs. [21–23]. In addition, note that in the above model we have neglected the effect of the Rashba spin-orbit interaction (RSOI). While this interaction is crucial for the emergence of a topologically nontrivial (i.e., D class) superconducting phase supporting Majorana zero-modes [41], here we will focus strictly on the topologically-trivial ground state. As we will show below, even in the absence of RSOI the competition between SU and FM interactions is already quite complex, and makes the topologically-trivial case very interesting in itself.

We note that since the total single-particle fermionic spin along z,

$$s_z = \frac{1}{2}\int_{-\frac{L_w}{2}}^{\frac{L_w}{2}} dx\, [\psi_\uparrow^\dagger(x)\psi_\uparrow(x) - \psi_\downarrow^\dagger(x)\psi_\downarrow(x)] \tag{4}$$

is a conserved quantity, which verifies $[s_z, H] = 0$, we can label the electronic eigenstates of H with $\sigma = \{\uparrow, \downarrow\}$ (note that in the presence of a RSOI, s_z is generically a nonconserved quantity, a fact that technically complicates the resolution of this problem). Therefore, we introduce the following Nambu spinors with well-defined spin projection along z,

$$\Psi_\uparrow(x) = \begin{pmatrix}\psi_\uparrow(x)\\ \psi_\downarrow^\dagger(x)\end{pmatrix}, \quad \Psi_\downarrow(x) = \begin{pmatrix}\psi_\downarrow(x)\\ \psi_\uparrow^\dagger(x)\end{pmatrix}, \tag{5}$$

related to each other via the charge-conjugation transformation $\Psi_{\bar\sigma}(x) = \mathcal{K}\tau_x\Psi_\sigma(x)$, where τ_x is the 2×2 Pauli matrix, and $\mathcal{K}$ is the complex conjugation operator. In terms of these spinors the Hamiltonian writes

$$H = \frac{1}{2}\sum_\sigma \int_{-\frac{L_w}{2}}^{\frac{L_w}{2}} dx\, \Psi_\sigma^\dagger(x)\mathcal{H}_{\mathrm{BdG},\sigma}(x)\Psi_\sigma(x), \tag{6}$$

where the Bogoliubov-de Gennes (BdG) Hamiltonian is defined as

$$\mathcal{H}_{\mathrm{BdG},\sigma} = \begin{pmatrix} -\frac{\hbar^2\partial_x^2}{2m} - \mu + \sigma h(x) & \sigma\Delta \\ \sigma\Delta & \frac{\hbar^2\partial_x^2}{2m} + \mu + \sigma h(x)\end{pmatrix}. \tag{7}$$

In this expression, the spin projection $\sigma = \uparrow (\downarrow)$ on the left-hand side corresponds to the $+(-)$ sign in the definition of the BdG matrix. Using the above charge-conjugation transformation, we note that the BdG Hamiltonian Eq. (7) verifies the following symmetry transformation

$$\mathcal{K}\tau_x\mathcal{H}_{\mathrm{BdG},\sigma} = -\mathcal{H}^*_{\mathrm{BdG},\bar\sigma}\mathcal{K}\tau_x, \tag{8}$$

and therefore, provided $\chi_\sigma(x)$ is a solution of the BdG eigenvalue equation

$$\mathcal{H}_{\mathrm{BdG},\sigma}(x)\chi_\sigma(x) = E_\sigma\chi_\sigma(x), \tag{9}$$

with eigenenergy E_σ, the transformed spinor $\chi_{\bar\sigma}(x) = \mathcal{K}\tau_x\chi_\sigma(x)$, is also a solution with eigenenergy $E_{\bar\sigma} = -E_\sigma$.

In what follows, we assume for simplicity the thermodynamic limit $L_w \to \infty$, and we focus on the features introduced by the magnitude and spatial dependence of $h(x)$, which is crucial for the rest of this paper. In addition, we assume the following step-like spatial profile for the exchange field:

$$h(x) = \begin{cases} -h_0 & \text{if } |x| < \frac{L}{2}, \\ 0 & \text{if } |x| \geqslant \frac{L}{2}, \end{cases} \tag{10}$$

which models a uniform FMI shell of length L in contact with the SE nanowire (see Fig. 1). This choice for $h(x)$ allows to split the problem into regions with either $|x| < \frac{L}{2}$ or $|x| > \frac{L}{2}$, with generic exponential solutions

$$\chi_\sigma(x) \sim \begin{pmatrix}u_\sigma(x)\\ v_\sigma(x)\end{pmatrix}e^{ikx}. \tag{11}$$

Linear combinations of Eq. (11), with appropriate coefficients and with allowed values of k for each region, must be built so that continuity of the total wavefunction and its derivative at the interfaces is satisfied. With this requirement, the solution of Eq. (9) is finally obtained.

Note that the BdG Hamiltonian (7) is even under space inversion $x \to -x$, and therefore its eigenstates must be even or odd under this transformation of coordinates. This symmetry allows to reduce the number of unknowns of the problem (i.e., coefficients of the linear combination). Replacing the above ansatz Eq. (11) into the BdG eigenvalue Eq. (9), and looking for localized solutions with energy within the gap $|E_\sigma| < \Delta$, we obtain the following expressions for the eigenstates belonging to the even-symmetry subspace:

$$\chi_{e,\sigma}\left(x > \frac{L}{2}\right) = A^e_{1\sigma}\begin{pmatrix}1\\ \sigma e^{-i\varphi_\sigma}\end{pmatrix}e^{-\kappa_\sigma x} + A^e_{2\sigma}\begin{pmatrix}1\\ \sigma e^{i\varphi_\sigma}\end{pmatrix}e^{-\kappa^*_\sigma x}, \tag{12}$$

$$\chi_{e,\sigma}\left(-\frac{L}{2} \leqslant x \leqslant \frac{L}{2}\right) = B^e_{1\sigma}\begin{pmatrix}1\\ \sigma e^{-\eta_\sigma}\end{pmatrix}\cos k_\sigma x + B^e_{2\sigma}\begin{pmatrix}1\\ \sigma e^{\eta_\sigma}\end{pmatrix}\cos\bar k_\sigma x, \tag{13}$$

and the following expressions for the odd-symmetry eigenfunctions:

$$\chi_{o,\sigma}\left(x > \frac{L}{2}\right) = A^o_{1\sigma}\begin{pmatrix}1\\ \sigma e^{-i\varphi_\sigma}\end{pmatrix}e^{-\kappa_\sigma x} + A^o_{2\sigma}\begin{pmatrix}1\\ \sigma e^{i\varphi_\sigma}\end{pmatrix}e^{-\kappa^*_\sigma x}, \tag{14}$$

$$\chi_{o,\sigma}\left(-\frac{L}{2} \leqslant x \leqslant \frac{L}{2}\right) = B^o_{1\sigma}\begin{pmatrix}1\\ \sigma e^{-\eta_\sigma}\end{pmatrix}\sin k_\sigma x + B^o_{2\sigma}\begin{pmatrix}1\\ \sigma e^{\eta_\sigma}\end{pmatrix}\sin \bar{k}_\sigma x, \tag{15}$$

where the coefficients $\{A^\nu_{1\sigma}, A^\nu_{2\sigma}, B^\nu_{1\sigma}, B^\nu_{2\sigma}\}$, with $\nu = \{e, o\}$, are unknowns to be fixed. In addition, in the above expressions we have introduced the parametrization

$$\cos\varphi_\sigma = \frac{E_\sigma}{\Delta}, \tag{16}$$

$$\cosh\eta_\sigma = \frac{E_\sigma + \sigma h_0}{\Delta}, \tag{17}$$

where we fix the definition of φ_σ to the interval $\varphi_\sigma \in (0, \pi]$. The phase variable φ_σ is associated to the Andreev reflection taking place at the interfaces $x_b = \pm L/2$. Note that the parametrization in Eq. (17) makes sense whenever the right-hand side is positive. If this condition is not satisfied, one can always use the symmetry Eq. (8) to send $E_\sigma \to -E_{\bar{\sigma}}$ and $\sigma \to \bar{\sigma}$. In addition, note that whenever $1 \leqslant (E_\sigma + \sigma h_0)/\Delta$ the parameter η_σ is purely real, while for $0 < (E_\sigma + \sigma h_0)/\Delta < 1$ it is purely imaginary. Finally, we have introduced the quantities

$$\kappa_\sigma \equiv -ik_F\sqrt{1 + \frac{2i}{k_F\xi}\sin\varphi_\sigma}, \tag{18}$$

$$k_\sigma \equiv k_F\sqrt{1 + \frac{2}{k_F\xi}\sinh\eta_\sigma}, \tag{19}$$

$$\bar{k}_\sigma \equiv k_F\sqrt{1 - \frac{2}{k_F\xi}\sinh\eta_\sigma}, \tag{20}$$

and the definition of the coherence length of the (proximity-induced) 1D superconductor $\xi = \hbar v_F/\Delta$. Notice also that the spatial dependence of the wavefunctions in the region $x < -L/2$ can be readily obtained by symmetry from the relations $\chi_{e,\sigma}(x) = \chi_{e,\sigma}(-x)$, and $\chi_{o,\sigma}(x) = -\chi_{o,\sigma}(-x)$.

We can intuitively understand the form of the scattering solutions in the regions $x > L/2$ and $x < -L/2$ in the limit $k_F\xi \gg 1$ (i.e., the semiclassical limit, see Sec. III A), where the momentum κ_σ in Eq. (18) can be expanded as $\kappa_\sigma \simeq -ik_F + \sin\varphi_\sigma/k_F\xi$, and the eigenfunctions Eqs. (12) and (14) take the form

$$\chi_{\nu,\sigma}\left(x > \frac{L}{2}\right) \approx \left[A^\nu_{1\sigma}\begin{pmatrix}1\\ \sigma e^{-i\varphi_\sigma}\end{pmatrix}e^{ik_F x} + A^\nu_{2\sigma}\begin{pmatrix}1\\ \sigma e^{i\varphi_\sigma}\end{pmatrix}e^{-ik_F x}\right] \times e^{-\frac{\sin\varphi_\sigma x}{\xi}}, \tag{21}$$

with $\nu = \{e, o\}$. In this way, it becomes evident that the component proportional to $A^\nu_{1\sigma}$ corresponds to a right-moving particle with momentum $+k_F$, while $A^\nu_{2\sigma}$ corresponds to a left-moving particle with momentum $-k_F$. In addition, the wavefunctions exponentially decay into the superconductor within a localization length $\lambda_{\rm loc} = \xi/\sin\varphi_\sigma = \xi/\sqrt{1 - (E_\sigma/\Delta)^2}$. These results are in complete agreement with Ref. [35], where the spectrum of SU-FM-SU Josephson junctions has been recently studied as a function of the length L of the FM region. However, in our case, the presence of a finite pairing gap Δ in the region $-L/2 < x < L/2$ (as opposed to the assumption $\Delta = 0$ in the FM region in that paper), gives rise to important differences, which we analyze below in Sec. III.

A. Continuity conditions at the interface

We now impose the continuity conditions on the wavefunction and its derivative at the boundary $x_b = L/2$,

$$\chi_{\nu,\sigma}(x_b^-) = \chi_{\nu,\sigma}(x_b^+), \tag{22}$$

$$\partial_x\chi_{\nu,\sigma}(x_b^-) = \partial_x\chi_{\nu,\sigma}(x_b^+). \tag{23}$$

Note that the same equations are obtained by symmetry at the other boundary $-x_b$. Inserting the solutions Eqs. (12)–(15), we can express the continuity equations in matrix form as

$$\begin{pmatrix}1 & \sigma e^{-i\varphi_\sigma}\\ \sigma e^{-i\varphi_\sigma} & 1\end{pmatrix}\begin{pmatrix}a^\nu_{1\sigma}\\ a^\nu_{2\sigma}\end{pmatrix} = \begin{pmatrix}1 & \sigma e^{-\eta_\sigma}\\ \sigma e^{-\eta_\sigma} & 1\end{pmatrix}\begin{pmatrix}F_\nu\left(\frac{k_\sigma L}{2}\right) & 0\\ 0 & F_\nu\left(\frac{\bar{k}_\sigma L}{2}\right)\end{pmatrix}\begin{pmatrix}b^\nu_{1\sigma}\\ b^\nu_{2\sigma}\end{pmatrix}, \tag{24}$$

$$-\begin{pmatrix}1 & \sigma e^{-i\varphi_\sigma}\\ \sigma e^{-i\varphi_\sigma} & 1\end{pmatrix}\begin{pmatrix}\kappa_\sigma & 0\\ 0 & \kappa^*_\sigma\end{pmatrix}\begin{pmatrix}a^\nu_{1\sigma}\\ a^\nu_{2\sigma}\end{pmatrix} = -s(\nu)\begin{pmatrix}1 & \sigma e^{-\eta_\sigma}\\ \sigma e^{-\eta_\sigma} & 1\end{pmatrix}\begin{pmatrix}k_\sigma G_\nu\left(\frac{k_\sigma L}{2}\right) & 0\\ 0 & \bar{k}_\sigma G_\nu\left(\frac{\bar{k}_\sigma L}{2}\right)\end{pmatrix}\begin{pmatrix}b^\nu_{1\sigma}\\ b^\nu_{2\sigma}\end{pmatrix}, \tag{25}$$

where we have conveniently redefined the unknown coefficients as

$$A^\nu_{1\sigma} \to e^{\kappa_\sigma L/2}a^\nu_{1\sigma} \quad B^\nu_{1\sigma} \to b^\nu_{1\sigma} \tag{26}$$

$$A^\nu_{2\sigma} \to \sigma e^{\kappa^*_\sigma L/2}e^{-i\varphi_\sigma}a^\nu_{2\sigma} \quad B^\nu_{2\sigma} \to \sigma e^{-\eta_\sigma}b^\nu_{2\sigma}, \tag{27}$$

in order to give these equations a more symmetric form. In addition, we have used the notation $s(\nu) = +1(-1)$ for $\nu = e(o)$, and $F_e(x) = G_o(x) \equiv \cos(x)$, $G_e(x) = F_o(x) \equiv \sin(x)$ for compactness.

In each subspace (even or odd) we have four equations and four unknowns. Eliminating the variables $(b^\nu_{1\sigma}, b^\nu_{2\sigma})^T$, and writing the equation for $(a^\nu_{1\sigma}, a^\nu_{2\sigma})^T$, we find from the

nullification of the corresponding determinant the following equations:

$$\frac{\cosh\eta_\sigma\cos\varphi_\sigma-1}{\sinh\eta_\sigma\sin\varphi_\sigma}=\begin{cases}\dfrac{|\kappa_\sigma|^2-(K_\sigma+\bar{K}_\sigma)\,\mathrm{Re}\,\kappa_\sigma+K_\sigma\bar{K}_\sigma}{(\bar{K}_\sigma-K_\sigma)\,\mathrm{Im}\,\kappa_\sigma} & \text{(even-symmetry subspace)},\\[2ex] \dfrac{|\kappa_\sigma|^2+(Q_\sigma+\bar{Q}_\sigma)\,\mathrm{Re}\,\kappa_\sigma+Q_\sigma\bar{Q}_\sigma}{(Q_\sigma-\bar{Q}_\sigma)\,\mathrm{Im}\,\kappa_\sigma} & \text{(odd-symmetry subspace)},\end{cases} \tag{28}$$

where we have defined the quantities

$$K_\sigma=k_\sigma\tan\left(\frac{k_\sigma L}{2}\right), \tag{29}$$

$$\bar{K}_\sigma=\bar{k}_\sigma\tan\left(\frac{\bar{k}_\sigma L}{2}\right), \tag{30}$$

$$Q_\sigma=k_\sigma\cot\left(\frac{k_\sigma L}{2}\right), \tag{31}$$

$$\bar{Q}_\sigma=\bar{k}_\sigma\cot\left(\frac{\bar{k}_\sigma L}{2}\right). \tag{32}$$

From Eq. (28), the eigenvalue E_σ for each subspace is finally obtained. This equation summarizes our main theoretical results. In the next Sec. III we analyze the numerical solution and different important limits.

B. Spin-changing quantum phase transitions

We now focus on the quantum phase transitions, which occur whenever one of the subgap states crosses E_F. In this section we follow the theoretical method of Ref. [35] to obtain a spin Friedel sum rule. We start by analyzing the spinors defined in Eq. (5), and consider the norm of the "up" spinor

$$q_\uparrow=\int_{-L_w/2}^{L_w/2}dx\,[\psi_\uparrow^\dagger(x)\psi_\uparrow(x)+\psi_\downarrow(x)\psi_\downarrow^\dagger(x)].$$

Recalling the definition of the single-particle s_z operator [see Eq. (4)], it is straightforward to associate these two quantities through the relation $q_\uparrow=2s_z-1$. Since s_z is a conserved quantity, so is the norm $q_\uparrow$ of the "up" Nambu spinors. This connection allows to interpret $q_\uparrow$ as an effective "conserved charge". Similar considerations allow to write the relation $q_\downarrow=-2s_z-1$. Due to the particle-hole relation Eq. (8), the information about s_z can be obtained with either $q_\uparrow$ or $q_\downarrow$. A more symmetric form involving both conserved charges is

$$s_z=\frac{q_\uparrow-q_\downarrow}{4}. \tag{33}$$

While redundant, this expression makes explicit that in the spin-symmetric case $q_\uparrow=q_\downarrow$, the net spin s_z must vanish ($s_z=0$).

We now return to Hamiltonian Eq. (7), and let us separate the effect of the proximity-induced Zeeman field, by writing it as $\mathcal{H}_{\mathrm{BdG},\sigma}=\mathcal{H}_{0,\sigma}+\mathcal{V}_\sigma$, where

$$\mathcal{H}_{0,\sigma}=\begin{pmatrix}-\frac{\hbar^2\partial_x^2}{2m}-\mu & \sigma\Delta\\ \sigma\Delta & \frac{\hbar^2\partial_x^2}{2m}+\mu\end{pmatrix}, \tag{34}$$

$$\mathcal{V}_\sigma=\begin{pmatrix}\sigma h(x) & 0\\ 0 & \sigma h(x)\end{pmatrix}. \tag{35}$$

In this form, we can interpret the effect of the exchange field as a "perturbation" on an otherwise homogeneous 1D superconductor represented by $\mathcal{H}_{0,\sigma}$. Therefore, the full and the unperturbed single-particle Green's functions in this problem are respectively defined as

$$\mathcal{G}_\sigma(z)=[z-\mathcal{H}_{0,\sigma}-\mathcal{V}_\sigma]^{-1}, \tag{36}$$

$$\mathcal{G}_{0,\sigma}(z)=[z-\mathcal{H}_{0,\sigma}]^{-1}, \tag{37}$$

From here, the total number of effective "up" charges $Q_\uparrow$ induced in the ground state due to the potential $\mathcal{V}_\sigma$, compared to the unperturbed homogeneous SU wire, can be computed as

$$\Delta Q_\uparrow=-\frac{1}{\pi}\mathrm{Im\,Tr}\int_{-\infty}^{\infty}d\epsilon\,n_F(\epsilon)\Delta\mathcal{G}_\uparrow(\epsilon+i\delta), \tag{38}$$

where $\Delta\mathcal{G}_\sigma(z)\equiv\mathcal{G}_\sigma(z)-\mathcal{G}_{0,\sigma}(z)$. At $T=0$, Eq. (38) can be easily computed from the well-known expression of the Friedel sum rule [42],

$$\Delta Q_\uparrow=\frac{1}{\pi}\int_{-\infty}^{0}d\epsilon\left[\frac{\partial\eta_\uparrow(\epsilon)}{\partial\epsilon}-\frac{\partial\eta_{0,\uparrow}(\epsilon)}{\partial\epsilon}\right] \tag{39}$$

$$=\frac{\eta_\uparrow(0)-\eta_{0,\uparrow}(0)}{\pi} \tag{40}$$

where we have defined the phase shifts [35,42],

$$\eta_\sigma(\epsilon)=\mathrm{Im\,ln\,det}\,\mathcal{G}_\sigma(\epsilon+i\delta), \tag{41}$$

$$\eta_{0,\sigma}(\epsilon)=\mathrm{Im\,ln\,det}\,\mathcal{G}_{0,\sigma}(\epsilon+i\delta), \tag{42}$$

and where we have used that the phase shifts vanish in the limit $\epsilon\to\pm\infty$.

Since the system is noninteracting, the Green's function Eq. (36) can be written in terms of single-particle eigenstates $|\alpha,\sigma\rangle$, with α a generic label, as

$$\mathcal{G}_\sigma(z)=\sum_\alpha\frac{|\alpha,\sigma\rangle\langle\alpha,\sigma|}{z-E_{\alpha,\sigma}}. \tag{43}$$

Therefore, after simple algebra, and using the above relations and the fact that in the absence of magnetic field $s_z=0$ [see Eq. (33)], the *total* S_z of the ground state is

$$S_z=\frac{\Delta Q_\uparrow}{2}=\frac{1}{2}\left[\sum_\alpha\Theta(-E_{\alpha,\uparrow})-\sum_{\alpha'}\Theta\big(-E^0_{\alpha',\uparrow}\big)\right], \tag{44}$$

where $\Theta(\epsilon)$ is the unit-step function. The above expression allows to interpret the total S_z of the ground state as a function of the "up" Nambu spinors with energy below $E_F=0$, as compared to the (unperturbed) situation $h_0=0$. Since the effective charges are quantized in integer numbers, the total spin S_z can only change in discrete "jumps" of $1/2$ whenever

a subgap state with projection up crosses below E_F (note that we have defined dimensionless spin operators). This interpretation makes sense since the ground state becomes spin polarized when the exchange field h_0 becomes large enough [i.e., the Zeeman energy of up-spin electron is *decreased*, see Eqs. (3) and (10)].

III. RESULTS

We start this section by analyzing different limits of the general result given in Eq. (28). In particular, in Sec. III A we focus on the semiclassical limit, and in Sec. III B we study the atomic limit, where we recover the YSR results. In both cases, Eq. (28) reduces to well-known analytical results. Finally in Sec. III C we show results corresponding to intermediate regimes, obtained by solving numerically Eq. (28).

A. Semiclassical limit

Generally speaking, the semiclassical limit is verified when E_F is the largest scale of the problem [43]. In particular, the condition $E_F \gg \Delta$ (which is very well satisfied in most experimental systems) can be expressed as $k_F\xi \gg 1$, recalling that after linearization of the normal quasiparticle dispersion, i.e., $\epsilon_{k,\sigma} \simeq \pm\hbar v_F k$, where the $+(-)$ sign corresponds to right-(left-)movers, the Fermi energy can be approximated as $E_F \simeq \hbar k_F v_F$. In this case, Eqs. (18)–(20) reduce to

$$r_\sigma \equiv \frac{\kappa_\sigma}{k_F} \simeq -i + \frac{\sin\varphi_\sigma}{k_F\xi}, \tag{45}$$

$$\zeta_\sigma \equiv \frac{k_\sigma}{k_F} \simeq 1 + \frac{\sinh\eta_\sigma}{k_F\xi}, \tag{46}$$

$$\bar{\zeta}_\sigma \equiv \frac{\bar{k}_\sigma}{k_F} \simeq 1 - \frac{\sinh\eta_\sigma}{k_F\xi}, \tag{47}$$

to leading order in $\mathcal{O}(k_F\xi)^{-1}$, and Eq. (28) becomes

$$\frac{\cosh\eta_\sigma\cos\varphi_\sigma - 1}{\sinh\eta_\sigma\sin\varphi_\sigma} \simeq s(\nu)\frac{1+\tan\left(\frac{k_F L\zeta_\sigma}{2}\right)\tan\left(\frac{k_F L\bar{\zeta}_\sigma}{2}\right)}{\tan\left(\frac{k_F L\zeta_\sigma}{2}\right)-\tan\left(\frac{k_F L\bar{\zeta}_\sigma}{2}\right)},$$
$$= s(\nu)\cot\left(\frac{L\sinh\eta_\sigma}{\xi}\right), \tag{48}$$

where we have used the trigonometric identity $\tan(x+y) = (\tan(x)+\tan y)/(1+\tan x\tan y)$. In general this transcendental equation cannot be solved analytically. However, in the regime of parameters $E_F \gg h_0 \gg \Delta$, where the exchange field h_0 is much larger than Δ, we can write $\cosh\eta_\sigma \approx \sinh\eta_\sigma \approx |\frac{h_0}{\Delta}| \gg 1$ [see Eqs. (16) and (17)], and Eq. (48) reduces to $\cot\varphi_\sigma = s(\nu)\cot(Lh_0/\hbar v_F)$. Equivalently we can write this result as

$$\arccos\left(\frac{E_\sigma}{\Delta}\right) = \begin{cases} \dfrac{LE_\sigma}{\hbar v_F} + \sigma\dfrac{Lh_0}{\hbar v_F} + 2n\pi, & \text{(even)} \\ \dfrac{LE_\sigma}{\hbar v_F} + \sigma\dfrac{Lh_0}{\hbar v_F} + (2n+1)\pi. & \text{(odd)} \end{cases} \tag{49}$$

This result can be interpreted as a semiclassical Bohr-Sommerfeld quantization condition for particles, which perform a complete a closed loop in the region $-L/2 < x < L/2$ [43]. In particular, it exactly coincides with theoretical results obtained for SU-FM-SU Josephson junctions with a normal (i.e., $\Delta = 0$) FM region [33–35], the only difference being that within our theoretical treatment, we can distinguish the symmetry of the solutions. The similarity of these results can be rationalized noting that a SU-FM-SU junction where the FM region is normal, corresponds to taking the limit $h_0 \gg \Delta$ in our Eq. (48) while keeping the ratio E_σ/Δ finite (since E_σ corresponds to a subgap state, it is always bounded by Δ), thus resulting in Eq. (49). This shows that our Eq. (28) is a generic relation describing different situations regardless of the magnitude of the ratio h_0/Δ.

B. YSR-impurity limit

We now consider the atomic limit in which the exchange profile becomes point-like, $L \to 0$, while $h_0 \to \infty$, in such a way that the product $Lh_0 = J = \text{const}$. Under these assumptions the magnetic barrier becomes a delta function and the Hamiltonian in Eq. (3) can be written as

$$H_Z \approx -J\int_{-\infty}^{\infty} dx\,\delta(x)[\psi_\uparrow^\dagger(x)\psi_\uparrow(x) - \psi_\downarrow^\dagger(x)\psi_\downarrow(x)]. \tag{50}$$

This is the usual model used in the seminal papers on YSR states [5–7]. In this case, it is easy to see that the odd-symmetry solutions decouple from the above Hamiltonian (50) as they vanish at $x = 0$, and only even solutions can couple to the delta potential.

As in the previous section, note that the limit $h_0 \to \infty$ implies $\cosh\eta_\sigma \approx \sinh\eta_\sigma \approx |\frac{h_0}{\Delta}| \gg 1$. However, the limit $h_0 \to \infty$ is not compatible with the semiclassical approach, as it violates the requirement $h_0 \ll E_F$. Therefore we cannot use here our previous Eq. (49). Instead, we must first take the limit $\eta_\sigma \gg 1$ together with the limit $L \to 0$, which applied to Eqs. (19) and (20) yield

$$k_\sigma \to k_F\sqrt{\frac{2h_0}{\hbar v_F k_F}}, \tag{51}$$

$$\bar{k}_\sigma \to ik_F\sqrt{\frac{2h_0}{\hbar v_F k_F}}. \tag{52}$$

In addition Eqs. (29)–(32) become

$$K_\sigma \to \frac{k_F h_0 L}{\hbar v_F} = k_F\rho_0 J, \tag{53}$$

$$\bar{K}_\sigma \to -\frac{k_F h_0 L}{\hbar v_F} = -k_F\rho_0 J, \tag{54}$$

where the expressions for the density of states per spin of 1D quasiparticles at the Fermi energy $\rho_0 = 1/\hbar v_F$, and the exchange coupling $J = h_0 L$, have been used. Replacing these expressions into Eq. (28) for the even-symmetry solutions, we obtain

$$\sigma\frac{E_\sigma^e}{\sqrt{\Delta^2 - (E^e)_\sigma^2}} = \frac{1-(\rho_0 J)^2}{(2J\rho_0)}. \tag{55}$$

From this expression, we can easily solve for E_σ^e

$$\frac{E_\sigma^e}{\Delta} = \sigma\frac{1-(\rho_0 J)^2}{1+(\rho_0 J)^2}, \tag{56}$$

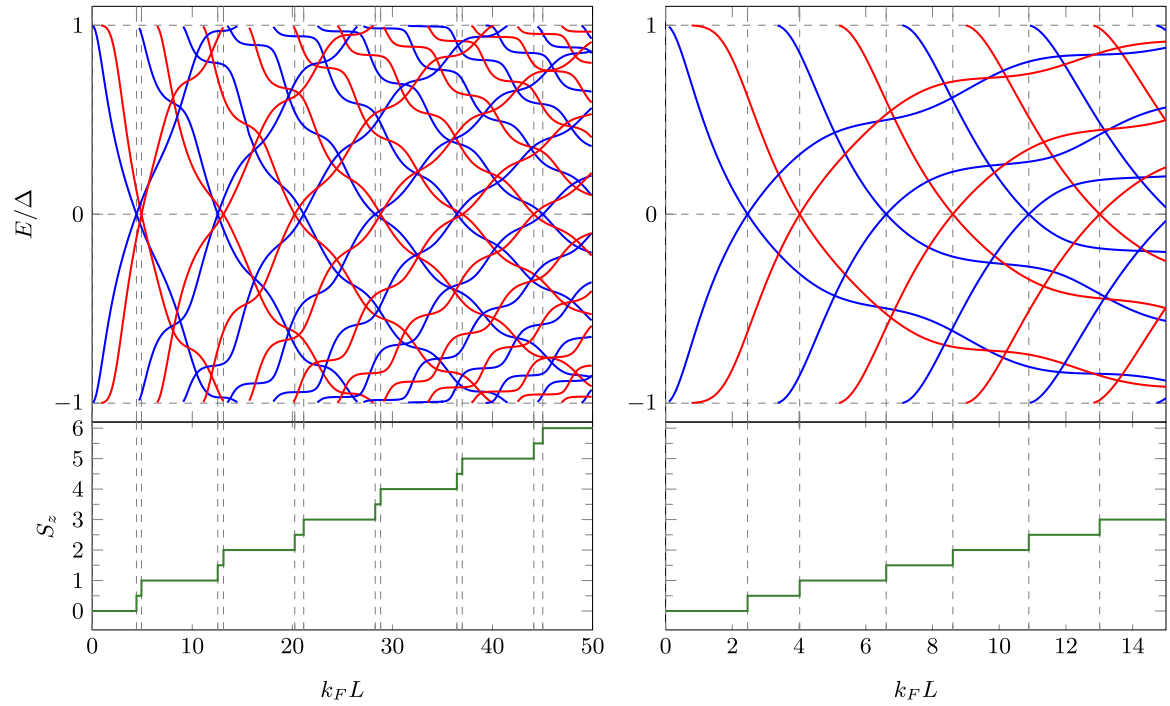

FIG. 2. Energy of the spin-polarized Andreev bound states (upper panel) and total spin S_z(lower panel) as a function of $k_F L$, for $k_F\xi = 7.8$ and $h_0/\Delta = 3.0$ (left panel) and $k_F\xi = 3.4$ and $h_0/\Delta = 2.1$ (right panel). Blue and red colors correspond to even and odd states respectively. Lines starting from the top gap edge at positive energy $E/\Delta = 1$ (bottom gap edge at negative energy $E/\Delta = -1$) correspond to up (down) spin projections of the states. For smaller values of $k_F L$ (right panel), plateaus corresponding to regions of integer and half-integer spin are more separated and might become easier to observe in experiments.

which is the well-known expression for the energy of YSR-impurity subgap level [1,5–7] . This result indicates that any finite value of J produces a YSR in-gap state. This type of subgap YSR states has been observed in several STM experiments on atomic magnetic adsorbates on superconducting substrates [30,44–48].

For completeness, and in order to illustrate the general scope of Eq. (28), here we also show the result for the YSR odd states for a small (but finite) L. Using similar approximations, we obtain the expression

$$\frac{E_\sigma^o}{\Delta} = \sigma \frac{1}{\sqrt{1+\left(\frac{\rho_0 J k_F^2 L^2}{6}\right)^2}}, \tag{57}$$

where it becomes evident that in addition to a finite value of J, a finite value of $k_F L$ is needed to observe an odd-symmetry subgap YSR state.

C. Spin-polarized subgap spectrum in generic cases

As stated in Sec. II, Eq. (28) implicitly defines the energy of the subgap states as a function of the parameters h_0/Δ, $k_F\xi$, and $k_F L$. These parameters can be directly or indirectly controlled in experiments, i.e., the parameter h_0 can be controlled by modifying the FMI material, the length L of the FMI region can be modified varying the length L_w of the semiconductor via vapor-liquid-solid (VLS) method and subsequent evaporation of the FMI material [21], and the parameter k_F in the semiconductor can be varied by changing the SE material or by introducing external gates to modify the chemical potential μ. Therefore, due to this high degree of tunability, hybrid heterostructures of this kind might offer a unique platform to produce and control engineered subgap states. Probably the easiest way to experimentally control the subgap electronic structure is by producing different devices with the same FMI material and different lengths L. Therefore, in this section we show the numerical solutions of Eq. (28) with fixed parameters h_0/Δ and $k_F\xi$ (which control the "operation regime" of the device), and calculate both the energy dependence of the even- and odd-symmetry ABS, and the total spin S_z of the ground state of device as a function of L (i.e., dimensionless variable $k_F L$).

Generally speaking, the overall evolution of the ABS spectrum from $L = 0$ to $L \to \infty$ is quite complex and deserves a detailed explanation. As shown in Fig. 2, as the parameter $k_F L$ increases, more and more subgap states emerge from the gap edges. This behavior is reminiscent of a quantum particle in a square-well potential, typically taught in introductory quantum mechanics courses [49], where increasing the width L of the well increases the number of allowed bound states. In our case, the emergence of new ABS as $k_F L$ increases can be intuitively understood in terms of a competition between superconductivity and magnetic field: The magnetic field tends to break Cooper pairs and to locally disrupt superconductivity in the magnetic region by introducing spin-polarized subgap states that become macroscopic in number for large L, eventually populating the whole gap.

We note that for any finite L, even- and odd-symmetry states are generically nondegenerate (except at isolated

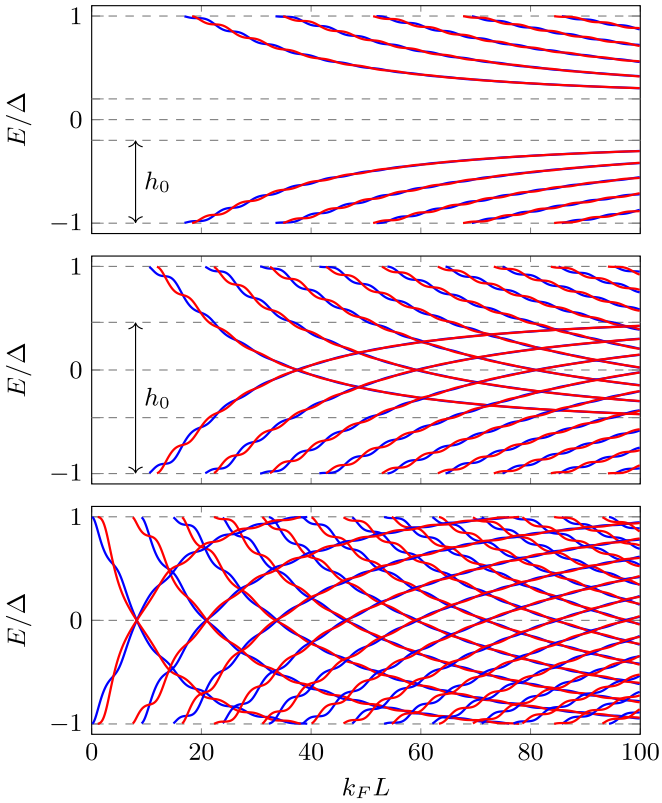

FIG. 3. Energy of the spin-polarized Andreev bound states as a function of $k_F L$ for the three different values of h_0 ($h_0/\Delta = 0.8$, 1.54, 2.2 for the lower, middle, and upper panels) and $k_F\xi = 8.2$. Blue and red colors correspond to even and odd states respectively. Lines starting from negative (positive) energies correspond to down (up) spin projections of the state. Note that the value of h_0/Δ sets the asymptotic limit for the Andreev states and is crucial to determine the overall subgap spectrum.

points). However, as it is clear from Figs. 2 and 3, their energy difference (evidenced as oscillations of the blue and red lines around the semiclassical value) decreases very rapidly and the solutions become degenerate in the limit $L \to \infty$. This transition from nondegenerate YSR states in the limit $L \to 0$, to double degenerate ABS states for $L \to \infty$ has been discussed in previous papers on ballistic SU-FM-SU junctions [19,33–35], and in the case of extended Shiba impurities in 1D nanowires [50]. It is also clearly visible in Fig. 2, and more dramatically in Fig. 3 below. In our 1D geometry, this degeneracy in the limit $L \to \infty$ can be intuitively understood by linearizing the spectrum around the Fermi energy, and expressing the original fermionic operators in terms of right- and left-moving fields slowly varying in the scale of k_F^{-1} [51], i.e., $\psi_\sigma(x) \approx e^{ik_F x}\psi_{R,\sigma}(x) + e^{-ik_F x}\psi_{L,\sigma}(x)$. The slowly-varying fields $\psi_{R,\sigma}(x)$ and $\psi_{L,\sigma}(x)$ are two independent chiral fermionic fields obeying the usual anticommutation relations, in terms of which the original Hamiltonian becomes [50]

$$H_{\rm w} \approx \sum_\sigma \int_{-\infty}^{\infty} dx[-i\hbar v_F \psi^\dagger_{R,\sigma}(x)\partial_x\psi_{R,\sigma}(x) + i\hbar v_F \psi^\dagger_{L,\sigma}(x)\partial_x\psi_{L,\sigma}(x)], \tag{58}$$

$$H_\Delta \approx \Delta \int_{-\infty}^{\infty} dx\,[\psi^\dagger_{R,\uparrow}(x)\psi^\dagger_{L,\downarrow}(x) + \psi^\dagger_{L,\uparrow}(x)\psi^\dagger_{R,\downarrow}(x) + \text{H.c.}], \tag{59}$$

$$H_{\rm Z} \approx -\int_{-\infty}^{\infty} dx\, h_0[\psi^\dagger_{R,\uparrow}(x)\psi_{R,\uparrow}(x) - \psi^\dagger_{R,\downarrow}(x)\psi_{R,\downarrow}(x) + \psi^\dagger_{L,\uparrow}(x)\psi_{L,\uparrow}(x) - \psi^\dagger_{L,\downarrow}(x)\psi_{L,\downarrow}(x)], \tag{60}$$

where oscillating terms proportional to $e^{\pm 2ik_F x}$ have been neglected as they cancel out in the limit $L \to \infty$ due to destructive interference. Defining the new chiral Nambu spinors

$$\Psi_{1,\sigma}(x) = \begin{pmatrix} \psi_{R,\sigma}(x) \\ \psi^\dagger_{L,\bar\sigma}(x) \end{pmatrix}, \quad \Psi_{2,\sigma}(x) = \begin{pmatrix} \psi_{L,\sigma}(x) \\ \psi^\dagger_{R,\bar\sigma}(x) \end{pmatrix}, \tag{61}$$

the Hamiltonian of the system can be expressed in terms of two decoupled chiral sectors

$$H = \frac{1}{2}\sum_{\sigma=\uparrow,\downarrow}\sum_{j=1,2}\int_{-\infty}^{\infty} dx\, \Psi^\dagger_{j,\sigma}(x)\mathcal{H}_{j,\sigma}(x)\Psi_{j,\sigma}(x), \tag{62}$$

with the definitions of the chiral BdG Hamiltonians

$$\mathcal{H}_{j,\sigma} = \begin{pmatrix} (-1)^j i v_F\partial_x - \sigma h_0 & \sigma\Delta \\ \sigma\Delta & -(-1)^j i v_F\partial_x - \sigma h_0 \end{pmatrix}. \tag{63}$$

The Nambu spinors Eq. (61) define two independent chiral subspaces related by the inversion symmetry of the original Hamiltonian, i.e., under the space inversion operation $x \leftrightarrow -x$, the fermionic operators transform as $\psi_{L,\sigma}(x) \leftrightarrow \psi_{R,\sigma}(x)$, and consequently we conclude that $\Psi_{1,\sigma}(x) \leftrightarrow \Psi_{2,\sigma}(x)$, which must then be degenerate. In addition, the particle-hole transformation $\mathcal{K}\tau_x$ in this representation produces $\Psi_{1,\sigma}(x) \to \Psi_{2,\bar\sigma}(x)$, and therefore $\mathcal{H}_{1,\sigma} \to -\mathcal{H}_{2,\bar\sigma}$, implying that the solutions verify the particle-hole symmetry property $E_{1,\sigma} = -E_{2,\bar\sigma}$. Moreover, notice that assuming periodic boundary conditions, the problem can be solved with the solutions $\psi_{R,\sigma}(x) \sim e^{ikx}$ and $\psi_{L,\sigma}(x) \sim e^{-ikx}$, and the dispersion relation becomes $E_{1,\sigma}(k) = E_{2,\sigma}(k) = \pm\sqrt{(\hbar v_F k)^2 + \Delta^2} - \sigma h_0$. This allows to understand the emergence of the double degeneracy in the spectrum of subgap states. In addition, from here it is easy to see that a renormalized quasiparticle gap $2\Delta_{\rm ren} = 2|\Delta - h_0|$ is obtained.

In terms of the chiral Nambu spinors, the most general solution is the linear combination

$$\Psi_\sigma(x) = Ae^{ik_F x}\Psi_{1,\sigma}(x) + Be^{-ik_F x}\Psi_{2,\sigma}(x). \tag{64}$$

This form can be recovered by combining the degenerate even and odd solutions in Eqs. (13) and (15) in the semiclassical limit where $k_F\xi \gg 1$.

From the analysis of the linearized Hamiltonian, we conclude that the degeneracy in the limit $L \to \infty$ arises from the absence of chirality-breaking terms, i.e., terms $\sim\Psi^\dagger_{1,\sigma}(x)\Psi_{2,\sigma}(x)$ [e.g., single particle backscattering terms $\psi^\dagger_{R,\sigma}(x)\psi_{L,\sigma}(x)$ or Cooper-pairing channels $\psi^\dagger_{R(L),\uparrow}(x)\psi^\dagger_{R(L),\downarrow}(x)$ carrying momentum $\mp 2k_F$]. These terms are strongly suppressed due to rapidly oscillating exponentials $\sim e^{\pm 2ik_F x}$, which occur whenever the magnetic FMI region is uniform and its length L is much larger than k_F^{-1}. In other words, the product $k_F L$ must be $k_F L \gg 1$, consistent with our numerical results in Figs. 2 and 3. Only for small values

of $k_F L$, where this destructive interference is incomplete, residual couplings of the type $\sim\Psi^\dagger_{1,\sigma}(x)\Psi_{2,\sigma}(x)$ remain, and the degeneracy is lifted. Finally, we stress that the degeneracy in the limit $L \to \infty$ is a robust property to the presence of interactions, as shown in previous papers [50].

On the other hand, in the limit $L \to 0$ and for any finite value of the Zeeman field h_0, both (even and odd) solutions converge to $E_\sigma/\Delta \to \pm 1$, indicating that the FMI region is no longer relevant (i.e., it physically drops from the description). However, the behavior near $L = 0$ is quite different for each case: while the even-symmetry solution tends to $E_\sigma/\Delta \to 1$ as [see Eq. (56)]

$$\frac{E^e_\sigma}{\Delta} \approx \sigma\left[1 - 2\left(\frac{h_0 L}{\hbar v_F}\right)^2 \ldots\right], \tag{65}$$

from Eq. (57) we conclude that the odd solution behaves as

$$\frac{E^o_\sigma}{\Delta} \approx \sigma\left[1 - \frac{1}{2}\left(\frac{h_0 k_F^2 L^3}{6\hbar v_F}\right)^2 \ldots\right], \tag{66}$$

therefore approaching the gap edge much faster as $L \to 0$, as expected.

Besides the general features of the spectrum discussed up to this point, its evolution as L increases is strongly affected by the values of the parameters $k_F\xi$ and h_0/Δ. In the following sections we analyze their effects in more detail.

1. Effect of varying the parameter $k_F\xi$

This parameter can be considered as a "knob", which tunes the device from the semiclassical behavior ($k_F\xi$ large, see left panel in Fig. 2) into a "quantum" regime ($k_F\xi$ small, see right panel) where the spectrum is dominated by quantum oscillations. The hybrid heterostructure under study is promising in this sense since, due to the combination of materials (in particular, semiconductors with a much smaller k_F as compared to metals), it is in principle possible to experimentally control $k_F\xi$. In addition, k_F could be further modified by introducing external gates (through the modification of the chemical potential μ of the SE nanowire). To illustrate the dramatic changes in the spectrum as $k_F\xi$ varies, in Fig. 2 we show the numerically obtained subgap spectra as a function of $k_F L$ for $k_F\xi = 7.8$ and $h_0/\Delta = 3.0$ (left panel), for and $k_F\xi = 3.4$ and $h_0/\Delta = 2.1$ (right panel). Solid blue (red) lines correspond to even(odd)-symmetry solutions. Moreover, since we always assume $h_0 > 0$, solutions emerging from the top edge $E/\Delta = 1$ (bottom edge $E/\Delta = -1$) correspond to spin up (spin down) solutions. In addition, note the reflection symmetry of the solutions around the horizontal $E = 0$ axis, a consequence of the particle-hole symmetry of the BdG Hamiltonian, Eq. (8).

Upon decreasing $k_F\xi$, the subgap spectrum becomes much more intricate due to the enhanced even-odd energy-splitting, which results in an amplified oscillatory behavior of the ABS (we have reduced the range of $k_F L$ in the right panel for clarity in the figure). Unfortunately, in the regime $k_F\xi \sim 1$ no analytic expressions for the subgap ABS are possible, but qualitative considerations can be provided. In fact, the amplified oscillations can be traced back to the larger energy dependence of the momenta Eq. (18)–(20) as $k_F\xi$ decreases. Then, whereas for large $k_F\xi$ all these quantities converge to a static (i.e., energy-independent) value $\sim k_F$, the limit of small $k_F\xi$ produces a larger effect on the space dependence of the wave functions through the exponential factors in Eqs. (12)–(15). This in turn produces larger interference effects, and more pronounced splitting of the even-odd degeneracy.

This phenomenological behavior enables interesting possibilities, such as the chance to observe half-integer spin (and fermion parity-switching) quantum phase transitions in the ground state. To illustrate this effect, we show the ground-state S_z transitions in the bottom panels of Fig. 2 in each case. While for larger $k_F\xi$, the half-integer S_z steps are very narrow due to the almost-degenerate even-odd solutions (i.e., the even and odd solutions cross zero energy almost at the same value of $k_F L$), for smaller $k_F\xi$ the S_z transitions occur in well-defined half-integer steps. This behavior is well explained by the enhanced lifting of the even-odd degeneracy, which allows to observe one ABS crossing zero energy at a time.

2. Effect of varying the parameter h_0/Δ

In Fig. 3 we show the evolution of the subgap spectrum as a function of $k_F L$, for different values of the Zeeman field $h_0/\Delta = 0.8, 1.54$, and 2.2, and for a fixed relatively large value $k_F\xi = 8.2$, allowing to interpret these results in terms of the semiclassical approximation. Here we can clearly distinguish three qualitatively different regimes: (a) the "weak field" regime $h_0 < \Delta$ (top panel) where the ABS do not cross $E = 0$, (b) the "intermediate field" regime $\Delta < h_0 < 2\Delta$ (middle panel) where the ABS can eventually cross zero energy, and quantum phase transitions can be induced, and finally (c) the "strong field" ($2\Delta < h_0$) regime (bottom panel), where the ABS can be found anywhere in the region $-1 < E_\sigma/\Delta < 1$. In all cases, the value of h_0 determines the asymptotic limit to which the ABS approach for large L (see dashed black lines in Fig. 3). Below we briefly discuss the main features of the spectrum in each regime.

(a) Weak-field regime $0 < h_0 < \Delta$. This regime is characterized by a Zeeman field, which is not strong enough to destroy the superconducting gap. In this case none of the ABS is able to cross $E = 0$ and in the limit $L \to \infty$ they asymptotically approach the value $E_\sigma/\Delta \to \sigma(1 - h_0/\Delta)$ (see horizontal dashed black lines), and therefore a renormalized gap remains (see top panel in Fig. 3). More quantitatively, in the semiclassical limit [Eq. (48)] they obey the asymptotic expression valid for $k_F L \to \infty$,

$$\frac{E^\nu_\sigma}{\Delta} \simeq \sigma\left[1 - \frac{h_0}{\Delta} + \frac{\pi^2}{2}\left(\frac{\xi}{L}\right)^2\left(1 - \frac{s(\nu)\xi}{L}\sqrt{\frac{2\Delta}{h_0} - 1}\right)^2\right], \tag{67}$$

with $s(\nu) = 1(-1)$ for $\nu = e(o)$. From here, we can clearly see that whereas the even-odd averaged quantities (i.e., the semiclassical values) approach the asymptotic limit as L^{-2}, the energy difference between even and odd solutions (i.e., the amplitude of the oscillation around the semiclassical limit) decreases as L^{-3}, and the solutions become degenerate in the limit $L \to \infty$. On the other hand, the quasiparticle gap in the limit $L \to \infty$ is renormalized to $2\Delta_{\rm ren} = 2|\Delta - h_0|$,

consistent with our previous result using chiral fields. Note that this gap renormalization is quite specific to this device, and is not present, for instance, in the case of Ref. [35], where the magnetic region is normal and not superconducting, and in addition the system corresponds to a "short" SU-FM-SU junction with $L < \xi$, and therefore only few subgap states are allowed.

Another feature of the weak-field regime is that the ABS require a minimal length $L_{\min}$ to emerge in the subgap region. This can be easily understood in terms of Eq. (49), where a minimal magnetic phase, represented by the product $Lh_0/\hbar v_F$, must be accumulated in order to produce an observable in-gap ABS. Finally, concerning the spin quantum number of the ground state, since none of the ABS cross E_F, no SP-QPT are expected according to the results of Sec. II B and the value of the ground state spin remains a spin-singlet $S_z = 0$.

(b) Intermediate field regime. $\Delta < h_0 < 2\Delta$*:* In this case the Zeeman field h_0 is sufficiently strong to force the ABS to cross the Fermi level, eventually inducing SP-QPT (see middle panel in Fig. 3). The nth critical value $L_{c,n}$ can be obtained imposing the condition $E_\sigma = 0$ on the semiclassical approximation in Eq. (48),

$$L^{\nu}_{c,n} = \xi \frac{\arctan\left(-s(\nu) \mp \sqrt{\left(\frac{h_0}{\Delta}\right)^2 - 1}\right) + n\pi}{\sqrt{\left(\frac{h_0}{\Delta}\right)^2 - 1}}, \tag{68}$$

with $s(\nu) = 1(-1)$ for $\nu = e(o)$.

In this regime, the ABS follow the same asymptotic behavior as in Eq. (67), approaching $E_\sigma/\Delta \to \sigma(1 - h_0/\Delta)$, although the overall subgap spectrum is completely different due to the closing of the gap, and due to the overlap of the $E_\uparrow$ and $E_\downarrow$ spin-polarized spectrum as L increases beyond the first critical $L_{c,0}$. In fact, in the regime $L > L_{c,0}$ the quasiparticle gap becomes completely populated (and washed away) by subgap states. Moreover, we predict an accumulation of levels in the region $-\Delta + h_0 < E < \Delta - h_0$, which can eventually form a peak structure in the total density of states.

(c) Strong field regime $2\Delta < h_0$. Finally, in this regime (see bottom panel in Fig. 3), the asymptotic dashed lines fall within the continuum and it is no longer possible to obtain an analytic expression for the spin-polarized ABS behavior in the limit $L \to \infty$. As a result, the subgap ABS can be found anywhere in the subgap region $-1 < E_\sigma/\Delta < 1$. In addition, we note that the minimal length required to observe in-gap ABS has reduced to $L_{\min} \approx 0$.

IV. SUMMARY AND CONCLUSIONS

In this paper we have analyzed the subgap electronic properties in the one dimensional SE-SU-FMI heterostructure schematically depicted in Fig. 1, a novel physical system recently fabricated using molecular beam epitaxy techniques (MBE). The main motivation to study this type of hybrid systems is that, via a careful combination of different materials, the emergent characteristics can be completely different from those of the individual components, providing a way to build devices with tailored properties and specific functionalities. In particular, much of the experimental effort has focused on the realization of topological superconducting phases hosting Majorana zero modes, with possible applications in topological quantum computing [21–23]. A distinguishing feature of these heterostructures is the coexistence of antagonistic superconductor and ferromagnetic insulating layers over a finite and arbitrary length L in a semiconductor wire, a combination that confers unique spectral properties, which cannot be found in elemental materials in nature.

In particular, we have modelled the hybrid structure assuming noninteracting fermions in a one-dimensional single-channel nanowire under the effect of two proximity-induced interactions: a SU pairing and a space-dependent Zeeman exchange coupling [see Eqs. (1)–(3)]. We have solved the associated Bogoliubov-de Gennes equations and, by imposing standard continuity conditions on the wave functions, we have obtained an equation [Eq. (28)] defining the subgap ABS spectrum of the device. This single equation encodes our main theoretical results. We stress that our approach is equivalent to other works using the scattering-matrix formalism. We have analytically solved Eq. (28) in two paradigmatic limits: the semiclassical limit (Sec. III A) and the Yu-Shiba-Rusinov limit, typical of atomic magnetic moments interacting with a superconductor (Sec. III B). In both cases, we have been able to recover well-known analytical results, providing important sanity checks for our theoretical results. As a consequence of the symmetries of the Hamiltonian (i.e., inversion $x \to -x$ and s_z spin symmetries), it was possible to classify the solutions into even- and odd-symmetry, and with s_z labels $\sigma = \uparrow, \downarrow$. In particular, we note that the even-odd classification, arising in the present case due to the inversion symmetry of the Hamiltonian, is nothing but the 1D analog of the classification in angular momentum eigenstates ℓ occurring in 3D spherically-symmetric Hamiltonians [7,28,29].

An important generic feature of the subgap ABS obtained in this paper is their spin polarized nature. We have studied the subgap spectrum of spin-polarized ABS as a function of different parameters, namely: the length of the magnetic region (through the dimensionless parameter $k_F L$), the strength of the Zeeman exchange induced by the FMI (parameter h_0/Δ), and the superconducting coherence length (parameter $k_F\xi$). We stress that each one of these parameters could in principle (directly or indirectly) be controlled in experiments. However, due to its potential relevance for on-going experimental efforts, we have in particular focused our study on the evolution of the subgap spectrum as a function of the length L (i.e., as it is probably the easiest parameter to vary in experiments), for fixed parameters $k_F\xi$ and h_0/Δ. The parameter L can be controlled by, e.g., changing the experimental growing conditions of the semiconductor nanowires using the VLS growth method. In Figs. 2 and 3 we have analyzed the evolution of the subgap spectrum in terms of the parameter $k_F L$ for different values of h_0/Δ and $k_F\xi$. Roughly speaking, while $k_F\xi$ controls the "semiclassical vs quantum" operation regime of the device, and the magnitude of the even-odd energy separation, the parameter h_0/Δ essentially controls the energy separation of the $E_\uparrow$ and $E_\downarrow$ spin-polarized solutions, eventually enabling many interesting physical phenomena such as the possibility to observe multiple ABS crossing zero energy, the existence of multiple SP-QPTs in the device, quasiparticle gap renormalization $\Delta \to \Delta_{\text{ren}} = |\Delta - h_0|$ in the limit of large $k_F L$, etc.. An important conclusion here is that in order to

experimentally observe a quantum phase transition, the condition $h_0 > \Delta$ must be fulfilled.

Interpreting L as a "tunable" parameter has another theoretical advantage, as it enables to address the interesting fundamental question of how to connect two paradigmatic limits in SU-FM hybrid devices: the atomic limit ($k_F L \to 0$), where the physics is that of the well-known nondegenerate YSR states, and the ballistic limit ($k_F L \gg 1$) where the spectrum of the subgap ABS becomes double degenerate. Until very recently, these limits were treated as disconnected from each other. In Ref. [35] this issue was addressed in the particular case of SU-FM-SU junctions in the limit $L < \xi$. Here we have revisited this intriguing question for a different setup where such constraint does not exist, and have studied the evolution of the subgap spectrum as a function of L. The above-mentioned symmetry classification into even and odd solutions is critically important to allow the interpretation of the degeneracy in the limit $k_F L \to \infty$ as an "even-odd degeneracy". At the same time, it enables to explain the degeneracy lifting in the limit $L \to 0$, where only even states prevail in the subgap region of energies. Using an approximate model of one-dimensional fermions with linearized dispersion, we have provided a simple picture where the even-odd degeneracy naturally emerges as a consequence of destructive interferences of terms $e^{\pm i2k_F x}$ arising from single-particle backscattering mechanisms.

The continuous evolution of the subgap spectrum as a function of $k_F L$ allows a better understanding of previous experimental STM results on atomic magnetic adsorbates on superconducting substrates, where the subgap YSR states are usually interpreted in terms of a point-like magnetic moment [30,44–48]. While the delta-function limit is obviously a mathematical idealization, in terms of our model the observed YSR states can be rationalized assuming a finite value of $k_F L$ and a (more physically appealing) finite value of the atomic local field h_0. This is precisely the case if we note that for magnetic impurities (e.g., Fe, Co, or Mn atoms) deposited on top of bulk metallic S surfaces (e.g., Pb or Al), the spatial extension of the short-ranged Zeeman field can be estimated as the size of the d-shell orbitals $L \sim 1$ Å, while the Fermi wavevector of bulk superconductors (e.g., Pb) is $k_F \sim 1 - 2\times10^{10}$ m^{-1} (see Ref. [52]). This type of adsorbate/substrate combination yields a parameter $k_F L \sim 1$, which is within the regime where we recover observable subgap states (see Figs. 2 and 3). On the other hand, in 1D semiconductor heterostructures as those of Refs. [21–23], k_F is usually much smaller than in metallic superconductors. Measurements of the number of carriers from the Hall conductance R_H in 2D InGaAl quantum wells [53] yield the estimated value $k_F \sim 2.2\times10^7$ m^{-1}, three orders of magnitude smaller as compared to bulk Pb. This much smaller value of k_F allows for much larger, experimentally accessible values of L, while keeping values of h_0 also within experimental reach. All together, this combination makes these hybrid materials a much more versatile platform to control the spectrum of YSR/ABS subgap states.

To characterize the SP-QPTs occurring in the device, we have computed the value of the total S_z using a spin version of the Friedel sum rule {see Eq. (44) and also Ref. [35]}. We stress that these transitions are a generalization of the well-known "$0 - \pi$" transition occurring in atomic YSR impurities [25,54] or quantum dots coupled to superconductors [55–57]. From this perspective, the difference with respect to atomic systems is that instead of a single transition, actually multiple transitions can occur due to the finite extension L of the "impurity" and the many ABS states with different symmetry, which can eventually cross below E_F. Interestingly, we stress that the occurrence of these quantum phase transitions can be tuned varying the length L.

We now briefly address the effect of the Rashba spin-orbit interaction (RSOI) and disorder, which has been neglected in our paper. As mentioned previously, the RSOI was neglected to simplify the theoretical description of this (already quite complex and rich) problem. This interaction can drive the system into the topological superconductor class D [58,59], hosting Majorana zero modes at the ends (see e.g., Ref. [41] for a related setup), and in that case we expect qualitative changes with respect to the results presented here. In particular, in the presence of a RSOI, the spin s_z is no longer a good quantum number, and the resulting ABS become a linear combination of spin-up and spin-down Nambu spinors in Eq. (5). This fact technically complicates the theoretical analysis presented in this paper, as the BdG Hamiltonian becomes a 4×4 matrix instead of the simpler 2×2 matrix in Eq. (7). In addition, important qualitative differences emerge, e.g., the ground state cannot be classified according to its total Sz, and the spin Friedel sum rule presented in Sec. II B is no longer valid. For small but nonvanishing values of the RSOI parameter α_R we expect the ABS subgap spectrum to be modified due to the mixing of the spin branches depicted in Figs. 2 and 3, with the opening of avoided crossings and gaps proportional α_R. Concomitantly, the sharp steps in Fig. 2 signaling the SP-QPTs are expected to become smeared and continuous. Consequently, our results only apply to experimental SE-SU-FMI systems where the Rashba energy term $E_{\rm SOC} = \alpha_R^2 m^*/2$ is negligible compared to Δ and h_0. Regarding the effect of disorder in this setup, we note that it might be a relevant effect as a random disorder potential will eventually break the inversion symmetry of the model and might lift the predicted even-odd degeneracy in the limit $k_F L \gg 1$. However, we believe the energy-lifting effect might be weak in epitaxially-grown samples, where disorder is a relatively small effect.

Finally, concerning the possibility to experimentally detect the results predicted in this paper, we note that the spin-polarized ABS subgap spectrum in epitaxially-grown devices, as well as the eventual occurrence of the predicted SP-QPTs, is within experimental reach using present-day techniques. One of such techniques is electron-tunnelling transport. In particular, spin-dependent tunneling spectroscopy has revealed the presence of spin-polarized ABS, as shown in Ref. [23]. Such spin-polarized ABS spectrum is similar to the one obtained in our paper, and is experimentally revealed in the cotunnelling processes. Interestingly, in that reference, ABS can be gate tuned through the Fermi energy, which leads to a SP-QPT. Moreover, in that experiment, the fermion parity

of the ground state can be directly revealed as an even-odd effect in Coulomb-blockaded transport. Another experimental technique is microwave spectroscopy, as was shown recently in Ref. [60]. In that paper, microwave spectroscopy of Andreev states in superconducting weak links tailored in an InAs-Al (core-full shell) epitaxially grown nanowires was performed, and the results were interpreted as zero-field spin-split Andreev states. These experimental results show that some of the predictions in our paper could be tested in the laboratory. In particular, while it seems complicated to have direct experimental access to the total S_z in the device, detecting the SP-QPTs with enough resolution using the above-mentioned techniques might allow to infer the quantum S_z of the ground state.

ACKNOWLEDGMENTS

This work was partially supported by CONICET under Grant PIP 0792, UNLP under Grant PID X497, and Agencia I + D + i under PICT 2017-2081, Argentina. The authors are very grateful to Liliana Arrachea, Sebastián Bergeret, Saulius Vaitiekėnas, Rubén Seoane Souto, and Leandro Tosi for useful discussions and for pointing out important bibliographic references.

[1] A. V. Balatsky, I. Vekhter, and J.-X. Zhu, Rev. Mod. Phys. **78**, 373 (2006).
[2] B. W. Heinrich, J. I. Pascual, and K. J. Franke, Prog. Surf. Sci. **93**, 1 (2018).
[3] R. Pawlak, S. Hoffman, J. Klinovaja, D. Loss, and E. Meyer, Prog. Part. Nucl. Phys. **107**, 1 (2019).
[4] D.-J. Choi, N. Lorente, J. Wiebe, K. von Bergmann, A. F. Otte, and A. J. Heinrich, Rev. Mod. Phys. **91**, 041001 (2019).
[5] Y. luh, Acta Phys. Sin. **21**, 75 (1965).
[6] H. Shiba, Prog. Theor. Phys. **40**, 435 (1968).
[7] A. I. Rusinov, Zh. Eksp. Teor. Fiz. Pisma. Red. **9**, 146 (1969) [JETP Lett. **9**, 85 (1969)].
[8] S. Nadj-Perge, I. K. Drozdov, B. A. Bernevig, and A. Yazdani, Phys. Rev. B **88**, 020407(R) (2013).
[9] J. Klinovaja, P. Stano, A. Yazdani, and D. Loss, Phys. Rev. Lett. **111**, 186805 (2013).
[10] J. Li, H. Chen, I. K. Drozdov, A. Yazdani, B. A. Bernevig, and A. H. MacDonald, Phys. Rev. B **90**, 235433 (2014).
[11] S. Nadj-Perge, I. K. Drozdov, J. Li, H. Chen, S. Jeon, J. Seo, A. H. MacDonald, B. A. Bernevig, and A. Yazdani, Science **346**, 602 (2014).
[12] M. Ruby, F. Pientka, Y. Peng, F. von Oppen, B. W. Heinrich, and K. J. Franke, Phys. Rev. Lett. **115**, 197204 (2015).
[13] B. E. Feldman, M. T. Randeria, J. Li, S. Jeon, Y. Xie, Z. Wang, I. K. Drozdov, B. Andrei Bernevig, and A. Yazdani, Nat. Phys. **13**, 286 (2017).
[14] R. Pawlak, M. Kisiel, J. Klinovaja, T. Meier, S. Kawai, T. Glatzel, D. Loss, and E. Meyer, npj Quantum Inf. **2**, 16035 (2016).
[15] M. Ruby, B. W. Heinrich, Y. Peng, F. von Oppen, and K. J. Franke, Nano Lett. **17**, 4473 (2017).
[16] H. Kim, A. Palacio-Morales, T. Posske, L. Rózsa, K. Palotás, L. Szunyogh, M. Thorwart, and R. Wiesendanger, Sci. Adv. **4**, eaar5251 (2018).
[17] B. Jäck, Y. Xie, and A. Yazdani, Nat. Rev. Phys. **3**, 541 (2021).
[18] F. S. Bergeret, A. F. Volkov, and K. B. Efetov, Rev. Mod. Phys. **77**, 1321 (2005).
[19] M. Eschrig, Phil. Trans. R. Soc. A. **376**, 20150149 (2018).
[20] F. Hübler, M. J. Wolf, T. Scherer, D. Wang, D. Beckmann, and H. v. Löhneysen, Phys. Rev. Lett. **109**, 087004 (2012).
[21] Y. Liu, S. Vaitiekėnas, S. Martí-Sánchez, C. Koch, S. Hart, Z. Cui, T. Kanne, S. A. Khan, R. Tanta, S. Upadhyay *et al.*, Nano Lett. **20**, 456 (2020).
[22] S. Vaitiekėnas, Y. Liu, P. Krogstrup, and C. M. Marcus, Nat. Phys. **17**, 43 (2021).
[23] S. Vaitiekėnas, R. S. Souto, Y. Liu, P. Krogstrup, K. Flensberg, M. Leijnse, and C. M. Marcus, Phys. Rev. B **105**, L041304 (2022).
[24] E. Prada, P. San-Jose, M. W. A. de Moor, A. Geresdi, E. J. H. Lee, J. Klinovaja, D. Loss, J. Nygård, R. Aguado, and L. P. Kouwenhoven, Nat. Rev. Phys. **2**, 575 (2020).
[25] A. Sakurai, Prog. Theor. Phys. **44**, 1472 (1970).
[26] A. Costa, J. Fabian, and D. Kochan, Phys. Rev. B **98**, 134511 (2018).
[27] A. I. Rusinov, Zh. Eksp. Teor. Fiz. **56**, 2047 (1969).
[28] M. E. Flatté and J. M. Byers, Phys. Rev. B **56**, 11213 (1997).
[29] L. Arrachea, Phys. Rev. B **104**, 134515 (2021).
[30] S.-H. Ji, T. Zhang, Y.-S. Fu, X. Chen, X.-C. Ma, J. Li, W.-H. Duan, J.-F. Jia, and Q.-K. Xue, Phys. Rev. Lett. **100**, 226801 (2008).
[31] M. Ruby, Y. Peng, F. von Oppen, B. W. Heinrich, and K. J. Franke, Phys. Rev. Lett. **117**, 186801 (2016).
[32] D.-J. Choi, C. Rubio-Verdú, J. de Bruijckere, M. M. Ugeda, N. Lorente, and J. I. Pascual, Nat. Commun. **8**, 15175 (2017).
[33] F. Konschelle, F. S. Bergeret, and I. V. Tokatly, Phys. Rev. Lett. **116**, 237002 (2016).
[34] F. Konschelle, I. V. Tokatly, and F. S. Bergeret, Phys. Rev. B **94**, 014515 (2016).
[35] M. Rouco, I. V. Tokatly, and F. S. Bergeret, Phys. Rev. B **99**, 094514 (2019).
[36] C.-X. Liu, S. Schuwalow, Y. Liu, K. Vilkelis, A. L. R. Manesco, P. Krogstrup, and M. Wimmer, Phys. Rev. B **104**, 014516 (2021).
[37] R. Singh and B. Muralidharan, Commun. Phys. **6**, 36 (2023).
[38] S. Takei, B. M. Fregoso, H.-Y. Hui, A. M. Lobos, and S. Das Sarma, Phys. Rev. Lett. **110**, 186803 (2013).
[39] W. Chang, S. M. Albrecht, T. S. Jespersen, F. Kuemmeth, P. Krogstrup, J. Nygård, and C. M. Marcus, Nat. Nanotechnol. **10**, 232 (2015).
[40] P. Krogstrup, N. L. B. Ziino, W. Chang, S. M. Albrecht, M. H. Madsen, E. Johnson, J. Nygård, C. M. Marcus, and T. S. Jespersen, Nat. Mater. **14**, 400 (2015).
[41] J. D. Sau and P. M. R. Brydon, Phys. Rev. Lett. **115**, 127003 (2015).
[42] A. C. Hewson, *The Kondo Problem to Heavy Fermions* (Cambridge University Press, Cambridge, 1993).
[43] K. Duncan and B. Györffy, Ann. Phys. **298**, 273 (2002).

[44] A. Yazdani, B. A. Jones, C. P. Lutz, M. F. Crommie, and D. M. Eigler, Science **275**, 1767 (1997).
[45] M. Iavarone, G. Karapetrov, J. Fedor, D. Rosenmann, T. Nishizaki, and N. Kobayashi, J. Phys.: Condens. Matter **22**, 015501 (2010).
[46] S.-H. Ji, T. Zhang, Y.-S. Fu, X. Chen, J.-F. Jia, Q.-K. Xue, and X.-C. Ma, Appl. Phys. Lett. **96**, 073113 (2010).
[47] J. Bauer, J. I. Pascual, and K. J. Franke, Phys. Rev. B **87**, 075125 (2013).
[48] N. Hatter, B. W. Heinrich, M. Ruby, J. I. Pascual, and K. J. Franke, Nat. Commun. **6**, 8988 (2015).
[49] L. D. Landau and E. M. Lifshitz, *Quantum Mechanics: Non-Relativistic Theory* (Pergamon Press, Oxford, 1958).
[50] T. Bortolin, A. Iucci, and A. M. Lobos, Phys. Rev. B **100**, 155111 (2019).
[51] T. Giamarchi, *Quantum Physics in One Dimension* (Oxford University Press, Oxford, 2003).
[52] N. Ashcroft, N. Mermin, and D. Wei, *Solid State Physics* (Cengage Learning, Boston, 2016).
[53] M. Kjærgaard, Proximity induced superconducting properties in one and two dimensional semiconductors: Towards topological states of matter, Ph.D. thesis, Copenhagen University, 2015.
[54] K. J. Franke, G. Schulze, and J. I. Pascual, Science **332**, 940 (2011).
[55] J. Bauer, A. Oguri, and A. C. Hewson, J. Phys.: Condens. Matter **19**, 486211 (2007).
[56] R. S. Deacon, Y. Tanaka, A. Oiwa, R. Sakano, K. Yoshida, K. Shibata, K. Hirakawa, and S. Tarucha, Phys. Rev. Lett. **104**, 076805 (2010).
[57] E. J. H. Lee, X. Jiang, M. Houzet, R. Aguado, C. M. Lieber, and S. De Franceschi, Nat. Nanotechnol. **9**, 79 (2014).
[58] A. Altland and M. R. Zirnbauer, Phys. Rev. B **55**, 1142 (1997).
[59] S. Ryu, A. P. Schnyder, A. Furusaki, and A. W. W. Ludwig, New J. Phys. **12**, 065010 (2010).
[60] L. Tosi, C. Metzger, M. F. Goffman, C. Urbina, H. Pothier, S. Park, A. L. Yeyati, J. Nygård, and P. Krogstrup, Phys. Rev. X **9**, 011010 (2019).